Journal of
Manufacturing and Materials Processing

MDPI

Article

Effect of Rapid Solidification on the Structure and Properties of Ag–Cu–(Ti,Zr) Brazing Alloys for Metal–Ceramic Joining

Sofya Terekhova *, Alexander Ivannikov, Anton Abramov, Veronika Kirillova, Vladimir Mikhalchik, Alexander Bazhenov, Pavel Morokhov, Ivan Fedotov, Ivan Klyushin, Nikita Popov and Oleg Sevryukov

Department of Materials Science, National Research Nuclear University (MEPhI), Moscow 115409, Russia; aaivannikov@mephi.ru (A.I.); avabramov@mephi.ru (A.A.); vok11012002@gmail.com (V.K.); vvmikhalchik@mephi.ru (V.M.); aabazhenov@mephi.ru (A.B.); ivannikov7@rambler.ru (P.M.); ivfedotov@mephi.ru (I.F.); i348hob2@yandex.ru (I.K.); nspopov@mephi.ru (N.P.); onsevryukov@mephi.ru (O.S.)
* Correspondence: smterekhova@mephi.ru; Tel.: +7-(910)-459-12-02

Abstract

Four compositions of rapidly quenched ribbon brazing alloys based on Ag–Cu–Ti (Ag–26.5Cu–1.5Ti, Ag–25Cu–5Ti) and Ag–Cu–Zr (Ag–26.5Cu–1.5Zr, Ag–25Cu–5Zr) systems were produced. Initial ingots were synthesized by arc melting. Rapidly solidified ribbons, 50–100 μm thick, were then fabricated from homogenized ingots using a "Crystall-702" facility. A comparative analysis of the microstructure and phase composition of both the ingots and ribbons was conducted using scanning electron microscopy and X-ray diffraction. The analysis revealed the presence of Cu_4Ti and CuTi intermetallic compounds in the Ag–Cu–Ti alloys, and $AgCu_4Zr$ and Zr_2Cu in the Ag–Cu–Zr alloys. Rapid quenching was found to produce metastable structures and significantly refine the intermetallic phases. Microhardness measurements of the ingot and ribbon states demonstrated a substantial influence of the processing route on the mechanical properties. The tensile strength of the ingots was also evaluated. The wetting angles of the rapidly quenched alloy melts on 99% Al_2O_3 (alumina) ceramic substrates under vacuum were determined. All produced ribbons, except for the Ag–26.5Cu–1.5Zr composition, demonstrated adequate wettability. Thus, these materials are considered promising for further research into heat-resistant metal–ceramic joints.

Keywords: rapid quenching; Ag–Cu–Ti/Ag–Cu–Zr systems; microstructure; wettability; tensile strength; active brazing; metal–ceramic joints

Academic Editor: Dulce M. Rodrigues

Received: 13 February 2026
Revised: 23 February 2026
Accepted: 26 February 2026
Published: 3 March 2026

1. Introduction

The development of reliable metal–ceramic joints for vacuum, electronic, and power engineering applications represents a critical challenge in materials science [1]. These joints, which combine the high strength, corrosion resistance, and wear resistance of ceramics with the ductility and toughness of metals [2], serve as essential components in hermetic enclosures, insulators, and thermally stressed electronics. The established industrial standard, the multi-step molybdenum–manganese (Mo–Mn) process, requires preliminary ceramic metallization [3,4]. Its labor-intensive nature, however, has driven the search for alternatives, among which active metal brazing is considered the most promising. This single-step process employs brazing alloys doped with active elements (Ti, Zr) that promote ceramic wetting via redox reactions at the interface [5,6].

Brazing alloys based on the Ag–Cu–Ti and Ag–Cu–Zr systems are the most widely used for this purpose. Foundational research in this area [7] demonstrated that both Ti

and Zr, when added to the Ag–Cu eutectic, actively react with oxide and nitride ceramics to form interfacial reaction layers, with titanium-containing alloys generally exhibiting better wettability. For the Ag–Cu–Ti system, the primary reaction products with Al_2O_3 have been identified as titanium intermetallics and oxides, such as Ti_3Cu_3O, Ti_2O, and Ti_2Cu [8–12]. In zirconium-containing alloys, studies [13,14] show that a ZrO_2 layer forms at the ceramic interface, while intermetallic phases such as Cu_4AgZr precipitate within the bulk of the filler metal. Subsequent work [15–19] has focused on modifying Ag–Cu–Zr alloy compositions (e.g., with Sn, Al, or Ti additions) to enhance joint microstructure and strength, as well as on investigating the kinetics of zirconium segregation to the ceramic surface [20,21].

Despite the relative maturity of Ag–Cu–Ti and Ag–Cu–Zr filler alloys, comparative studies of these systems produced under identical conditions are lacking [22–24]. Such research would significantly expand the field of knowledge and potential applications. Moreover, detailed investigation of these systems will extend the applicability of mathematical models used to predict the behavior of both the filler alloys and the resulting metal–ceramic joints. Therefore, improving the accuracy of finite-element modeling for brazed alloys requires a detailed understanding of both the brazing alloy properties and the phases constituting the joint.

The benefits of rapid solidification, such as the formation of metastable structures with high homogeneity and fine phase dispersion, are well documented. For instance, in nickel-based brazes, this technique suppresses the formation of brittle intermetallics and improves joint strength [22,25]. When applied to the Ag–Cu–Ti/Zr systems, the melt-spinning technique could produce similarly refined microstructures.

Therefore, this work aims to produce and comprehensively investigate rapidly quenched ribbon brazing alloys with the following compositions (in wt.%): Ag–26.5Cu–1.5Ti, Ag–25Cu–5Ti, Ag–26.5Cu–1.5Zr, and Ag–25Cu–5Zr. The objectives of this study were to synthesize homogeneous master ingots; produce rapidly quenched ribbons and characterize their microstructure and phase composition using X-ray diffraction (XRD) and electron microscopy; determine the solidus and liquidus temperatures of the ribbons via differential scanning calorimetry (DSC); and analyze the microhardness and tensile strength of the obtained ingots. Finally, the wetting properties of melts produced from the rapidly quenched ribbons were evaluated on a 99% Al_2O_3 ceramic substrate.

Notably, the thermal shock resistance of joints made with rapidly quenched brazing alloys remains poorly characterized. Defined as the ability to maintain hermeticity and mechanical strength under cyclic thermal loading, thermal shock resistance is a critical parameter for many applications [26–30]. While data exist for joints made via traditional metallization routes [4], information on active-brazed joints—particularly those produced using rapidly quenched brazing alloy—is fragmentary. The results of this study establish a foundation for subsequent research, which will focus primarily on evaluating how the composition and microstructure of these rapidly quenched brazing alloys influence the thermal shock resistance and mechanical strength of brazed joints under thermal cycling conditions.

2. Materials and Methods

The compositions of the brazing alloys substrate materials considered in the work are presented in Table 1.

Master ingots (Table 1) were produced by induction melting in a “Crystall-702” unit. The charge materials consisted of copper, titanium, zirconium, and 99.99%-pure silver. Rapidly quenched brazing alloy ribbons, approximately 50–100 μm thick, were subse-

quently fabricated from these ingots using the flat-jet casting technique on the same "Crystall-702" facility. The estimated cooling rate during this process was 10^5–10^7 K/s.

Table 1. Composition of the brazing alloys and substrate materials.

Material	Composition, wt.%	Annealing Mode
AgCu1.5Zr AgCu5Zr AgCu1.5Ti AgCu5Ti	Ag–26.5Cu–1.5Zr Ag–25Cu–5Zr Ag–26.5Cu–1.5Ti Ag–25Cu–5Ti	730 °C for 5 h
99%Alumina	Al_2O_3–0.3MgO	–

The mechanical properties of the ingots were characterized by tensile strength and microhardness measurements. Tensile specimens of the required geometry (Figure 1) were cut from homogenized ingots using wire electrical discharge machining. Uniaxial tensile tests were performed on a UTS-111.2-50 universal testing machine (Test Systems, Ivanovo, Russia) at a crosshead speed of 1 mm/min, using self-aligning grips to minimize bending moments.

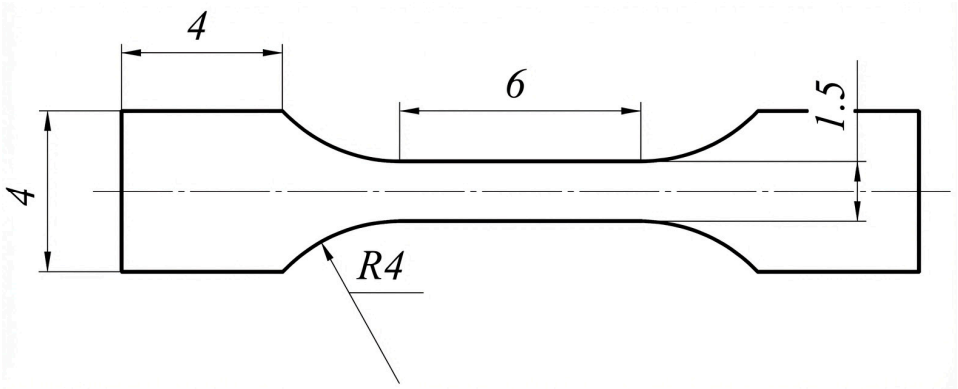

Figure 1. Tensile test specimens (dimensions in mm) [31].

The Vickers microhardness of the ingots was measured in both the as-cast and homogenized states (Table 1) using an FM-810 microhardness tester (Dealtek, Moscow, Russia).

To analyze the microstructure and composition of the brazed joints, cross-sectional specimens were prepared by mounting them in polymer resin, followed by grinding and polishing on a semi-automated LaboPol-5 machine (Struers ApS, Ballerup, Denmark) using water-based diamond suspensions and appropriate polishing cloths. The prepared cross-sections were examined using a Carl Zeiss EVO 50 scanning electron microscope (SEM) (Carl Zeiss AG, Oberkochen, Germany). The local composition was determined by energy-dispersive X-ray spectroscopy (EDX) using an INCA X–Act detector (Oxford Instruments plc, High Wycombe, England) at an accelerating voltage of 5 kV. The bulk phase composition of the ingots was analyzed via X-ray diffraction (XRD) on a DX-27mini diffractometer (Dandong Haoyuan Instrument, Dandong City, China) using Cu Kα radiation (λ = 1.5406 Å) equipped with a monochromator. Measurements were performed at 40 kV and 12 mA in the 2θ range of 20–90° with a step size of 0.03° and an exposure time of 1 s per step. Phase identification was carried out by comparing the obtained diffraction patterns with reference data from the ICDD Pdf-2 database and with published crystallographic data for the specific phases.

The thermal properties of the synthesized ribbons were analyzed using a Netzsch STA 409 CD thermal analyzer (Netzsch Erich Netzsch GmbH & Co, Selb, Germany). Each sample underwent two consecutive heating cycles up to 1100 °C at a constant rate of

20 °C/min under a protective atmosphere of high-purity argon (grade 6.0) flowing at 70 mL/min. Measurements were performed in a Netzsch Al_2O_3 DSC crucible (Netzsch Erich Netzsch GmbH & Co, Selb, Germany).

Wetting studies were performed on substrates of 99% Al_2O_3 ceramic (Table 1). Following GOST 23904-79 [32], brazing alloy samples with a volume of ~64 mm^3 (approximately 0.2 g) were prepared by cutting and spot-welding segments of the ribbon. These preforms were placed on the substrates and heated in the vacuum chamber of an EP–IRIS electric furnace designed for wetting experiments. The tests were conducted under a vacuum better than 1×10^{-3} Pa, with a heating rate of 5 °C/min up to a peak temperature of 1000 °C. Figure 2 presents the experimental temperature curve for the wetting experiments. The spreading process was monitored in situ, and images of the molten alloy on the Al_2O_3 ceramic were captured with a digital camera. The final wetting angles were measured from these images using KOMPAS–3D v19 x64 software. For each alloy composition, the contact angle was measured at least three times on the obtained droplet, and the average values are reported.

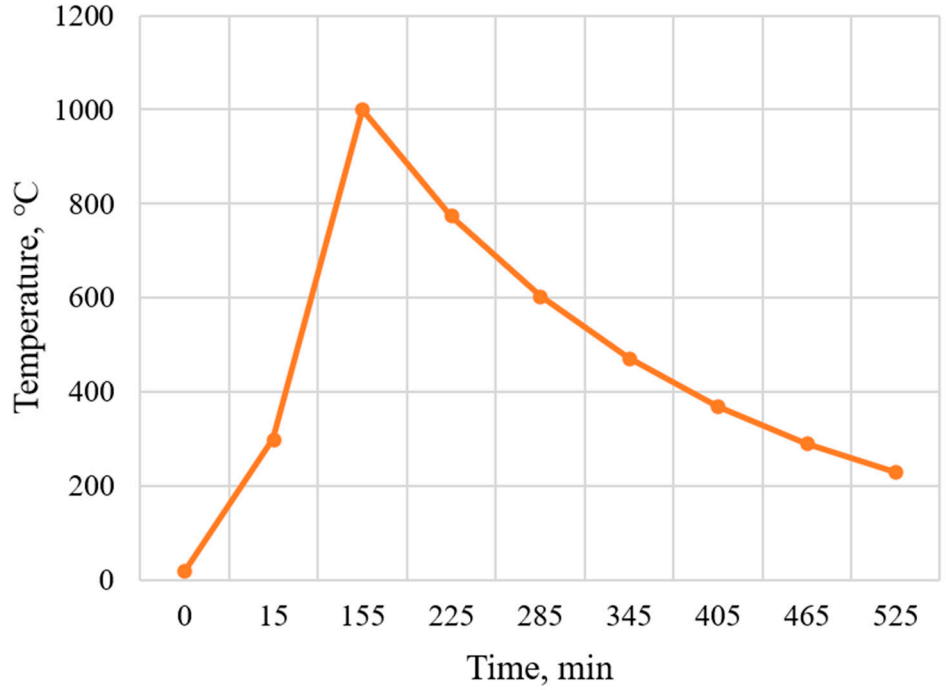

Figure 2. Heating and cooling curves for spreading and wetting experiments.

3. Results and Discussion

3.1. Characteristics of the Obtained Ingots

The microstructure of the ingot cross-sections before and after annealing is shown in Figure 3, with the corresponding microhardness values provided in the images. The increase in hardness observed for the AgCu1.5Ti ingot after annealing is attributed to a finer and denser distribution of intermetallic compounds.

Homogenization annealing at 730 °C for 5 h was performed to eliminate liquation inhomogeneity and bring the microstructure of the Ag–Cu–X (X = Ti, Zr) alloys closer to the equilibrium state.

The initial microstructure of the Ag–Cu–1.5Zr alloy (Figure 3a) consists of Cu–Zr intermetallic phases. After heat treatment, partial dissolution and spheroidization of the intermetallics occur, and the amount of the eutectic phase decreases, leading to the formation of more dispersed particles (Figure 3b). The highly alloyed Ag–Cu–5Zr alloy exhibits a structure composed of large dendrites (Figure 3c). Annealing causes their

refinement, forming finer, rounded precipitates, while the eutectic constituent almost completely disappears (Figure 3d). In both cases, copper from the eutectic is incorporated into the intermetallics, and the structure is transformed.

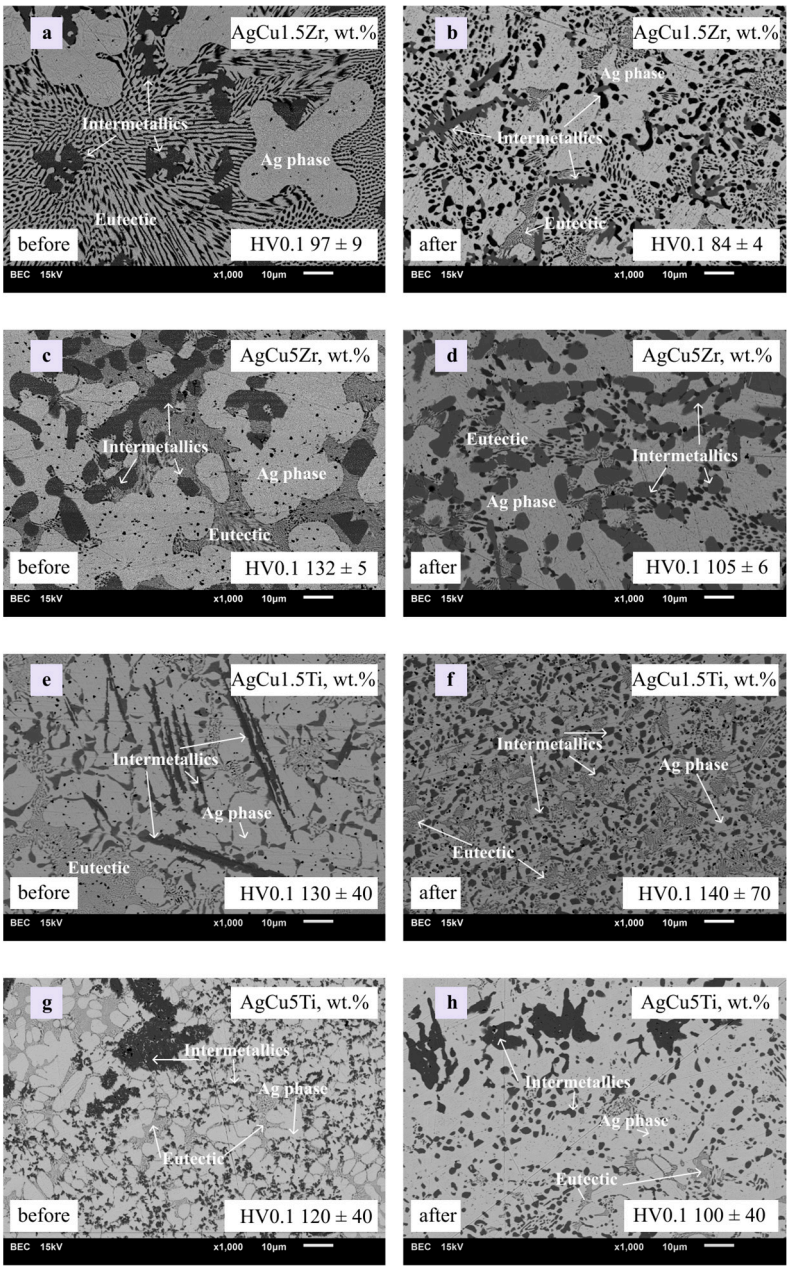

Figure 3. Microstructure of ingot cross-sections before and after annealing: (**a**,**c**,**e**,**g**)—as-cast state; (**b**,**d**,**f**,**h**)—annealed state.

In the initial state, the microstructure of the Ag–Cu–1.5Ti alloy is characterized by a fine network-like eutectic and dendritic clusters of Ti–Cu-based intermetallics (Figure 3e). Following annealing (Figure 3f), coagulation and spheroidization of these phases are observed, resulting in the formation of rounded precipitates within the silver matrix. The Ag–Cu–5Ti alloy exhibits an initially heterogeneous structure with large primary intermetallics (Figure 3g). Annealing leads to increased homogeneity, coagulation of fine phases, and the preservation of the large intermetallic particles (Figure 3h). Both compositions undergo microstructural transformation as copper from the eutectic is consumed by the growing intermetallic phases.

Thus, the selected homogenization regime enables the formation of a more uniform structure. The transformation mechanisms include spheroidization, coagulation, and dissolution of the intermetallic phases. The differences in the initial morphology of the intermetallics are primarily dictated by the thermodynamics of the respective binary systems.

The phase composition of the obtained ingots was studied using EDX and confirmed by XRD analysis. The investigation focused on the ingots with the highest content of the active element. The analysis confirmed the multiphase nature of the ingot structure. Micrographs of the brazing alloy structures containing 5 wt.% of the active element are presented in Figure 4.

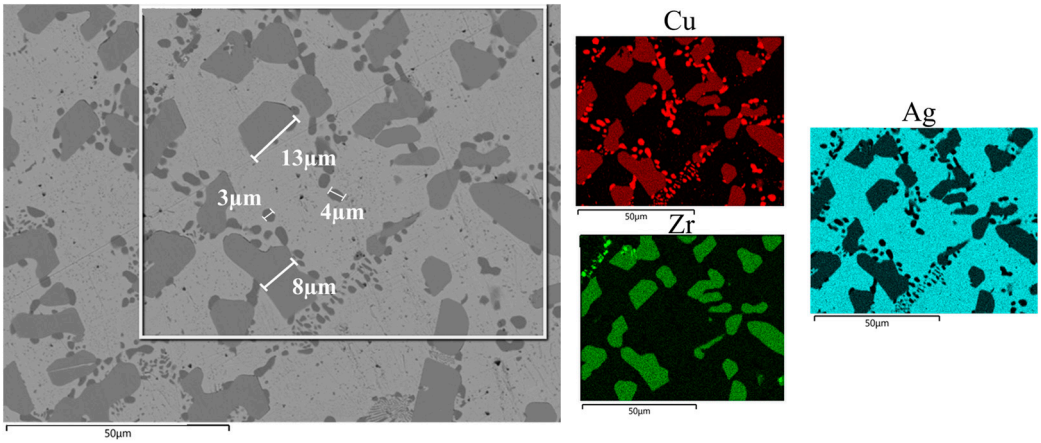

Figure 4. Element distribution map of AgCu5Zr.

The ingots consist of several phases. In the zirconium-containing ingot (Figure 4), the silver matrix contains large zirconium- and copper-rich structures, with copper accumulated at their boundaries. The zirconium-rich inclusions are relatively large, reaching up to 13 µm in size, while the copper-rich phases are more finely dispersed, with diameters of 4–5 µm.

The AgCu5Ti ingot (Figure 5) also features a silver matrix with uniformly distributed copper and copper–titanium intermetallic phases. The mesh structure is composed entirely of copper–titanium intermetallics, with inclusion sizes ranging from 1.5 to 12 µm. These phases are examined in more detail in the following section.

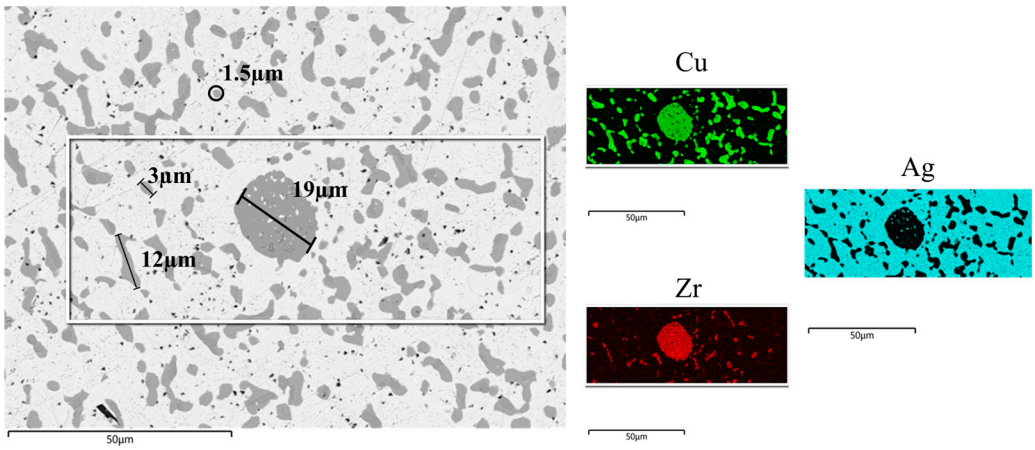

Figure 5. Element distribution map of AgCu5Ti.

The phase composition was investigated in greater detail using EDX (Table 2) and XRD (Figure 6c,d) analyses.

Table 2. EDX results for ingots.

Region	Content, wt. %			
	Ti	Cu	Ag	Zr
1	21.4	74.4	4.2	-
2	14.4	75.9	9.7	-
3	-	6.4	93.6	-
4	-	94.3	5.7	-
5	-	41.9	58.1	-
6	-	56.4	26.2	17.5
7	-	8.5	91.5	-

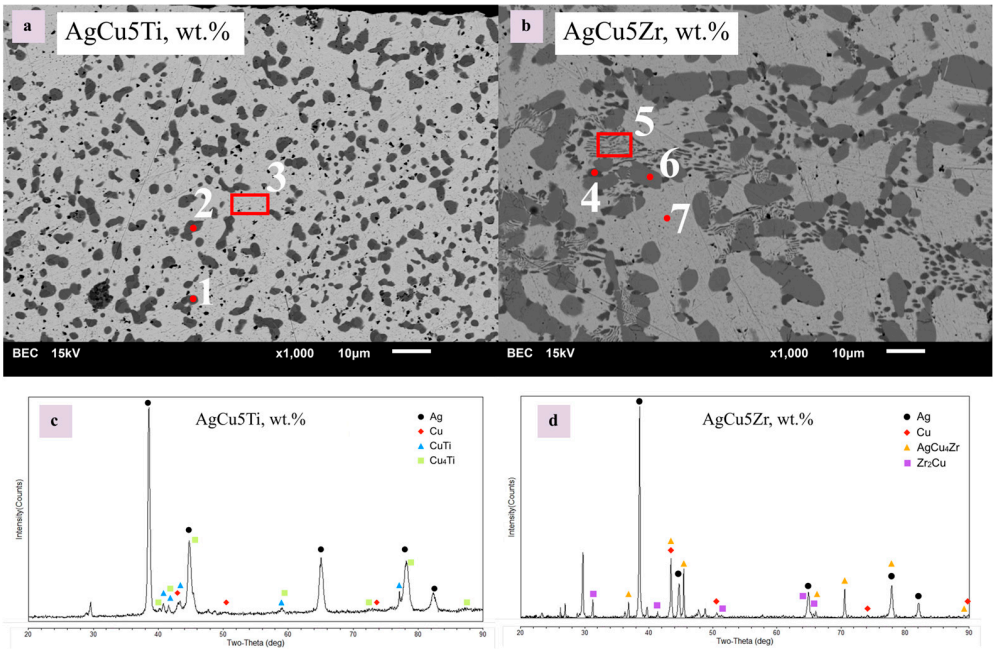

Figure 6. Phase analysis of the obtained ingots: (**a**,**b**)—EDX analysis; (**c**,**d**)—XRD spectra.

EDX analysis of the AgCu5Ti ingot (Figure 6a), the results of which are presented in Table 2, indicates the presence of a silver-based solid solution (Region 3) and Ti–Cu intermetallic compounds (Regions 1 and 2). According to the XRD analysis (Figure 6c), these phases correspond to the intermetallics CuTi and Cu_4Ti.

The AgCu5Zr ingot exhibits a more complex structure, as shown in Figure 6b. It consists of a silver-based solid solution (Region 7, Table 2), a copper-based solid solution (Region 4, Table 2), a distinct eutectic mixture (Region 5, Table 2), and zirconium-rich intermetallic compounds (Region 6) of the $AgCu_4Zr$ and Zr_2Cu types, as indicated by the XRD spectrum (Figure 6d). Although the phase diagram suggests the possible presence of an AgZr compound in the ingot composition, this was not confirmed by the XRD analysis.

The calculated properties of the relevant intermetallic compounds, taken from the literature, are summarized in Table 3.

Table 3. Properties of the observed intermetallic phases.

Phases	Space Group	B (GPa)	G (GPa)	B/G *	Reference
CuTi	P4/nmm	136.76	82.74	1.65	[33]
Cu_4Ti	I4/m	138.64	53.37	2.59	[33]
$AgCu_4Zr$	F-43m	–	–	–	[34]
Zr_2Cu	P4/nmm	111.00	46.00	2.41	[35]

* B (GPa)—bulk modulus; G (GPa)—shear modulus.

According to reference [36], the B/G ratio indicates material ductility: a value below 1.75 signifies brittle behavior, while a higher value indicates ductility. Based on this criterion, nearly all observed phases exhibit ductile behavior. However, the CuTi phase is brittle.

The mechanical properties of the ingots were also investigated via tensile testing. A total of five specimens of each type were prepared. The test results are presented in Figure 7, and SEM images of the fracture surfaces are shown in Figure 8.

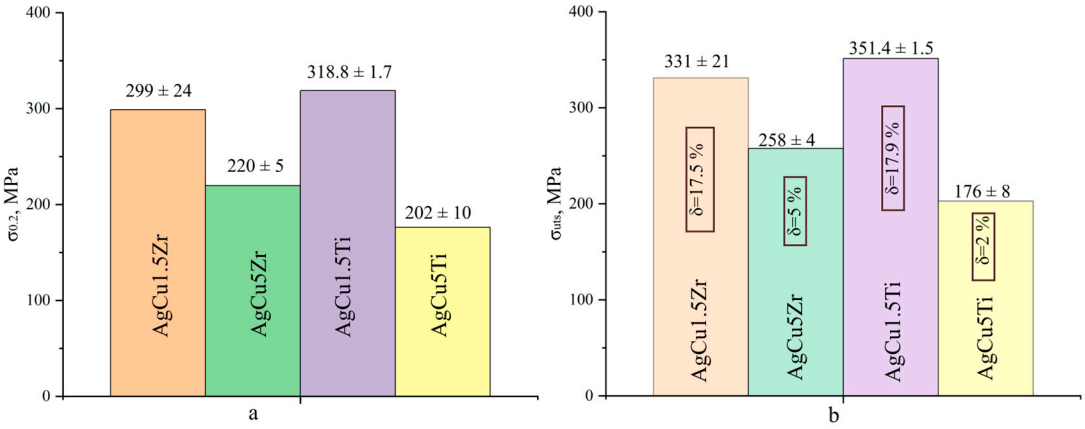

Figure 7. Tensile strength of ingots: (**a**)—yield strength; (**b**)—ultimate tensile strength.

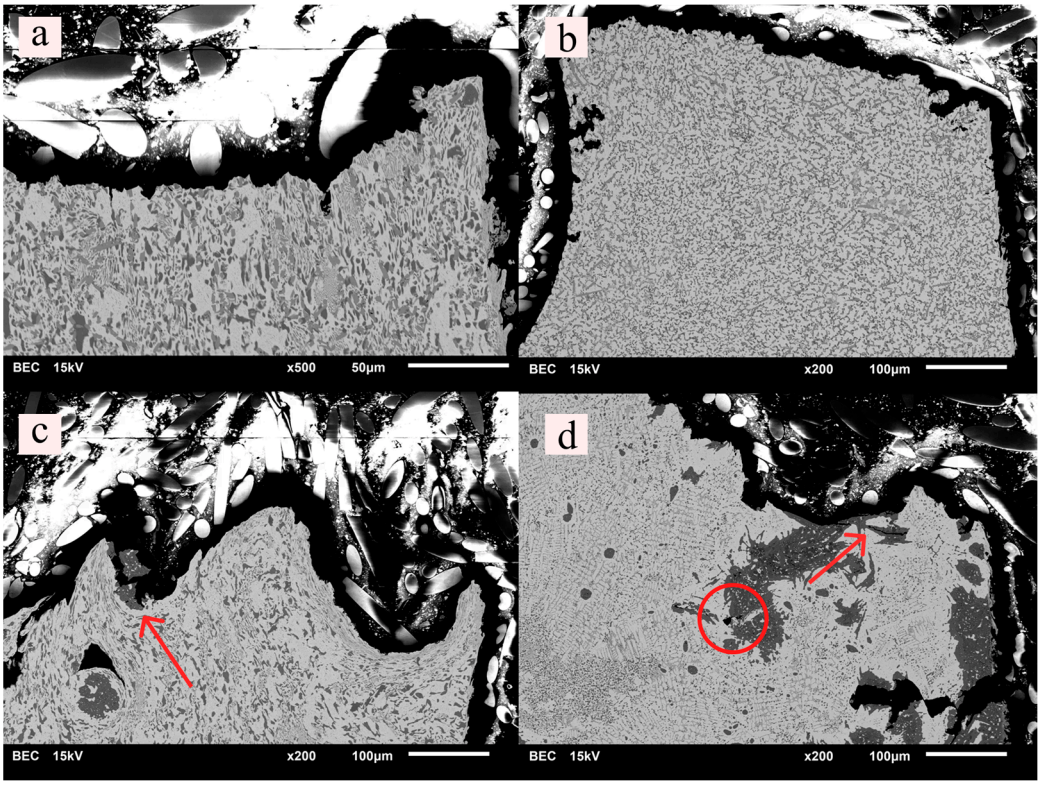

Figure 8. SEM images of the fracture surface: (**a**)—AgCu1.5Zr; (**b**)—AgCu5Zr; (**c**)—AgCu1.5Ti; (**d**)—AgCu5Ti. Arrows/round indicate destroyed intermetallics.

Ag–Cu–1.5Zr exhibits the following properties: $\sigma_{0.2}$ = 299 ± 24 MPa, σ_{uts} = 331 ± 21 MPa, δ = 17.5%. Fracture occurs uniformly through the intermetallics (Figure 8a). Increasing Zr content to 5% reduces both strength (σ_{uts} = 258 ± 4 MPa) and ductility (δ = 5%) (Figure 8b).

Ag–Cu–1.5Ti demonstrates the highest strength among the studied alloys: $\sigma_{0.2}$ = 318.8 ± 1.7 MPa, σ_{uts} = 351.4 ± 1.5 MPa, δ = 17.9%. SEM images of the fracture

surfaces (Figure 8c) reveal cracked and pulled-out intermetallic particles, suggesting a more brittle matrix–particle interface. However, the high ductility implies that such defects are not critical. At 5% Ti, embrittlement occurs: σ_{uts} = 176 ± 8 MPa, δ = 2%. The $\sigma_{uts} < \sigma_{0.2}$ ratio indicates brittle failure within the elastic regime (Figure 8c). The test results are largely determined by the content and nature of the intermetallic phases. The alloy with the highest titanium content, which exhibited the most brittle phases (Table 2), correspondingly showed the poorest mechanical performance, confirming this correlation.

3.2. Characteristics of the Ribbons

The composition of the obtained rapidly quenched ribbons was also examined using EDX analysis, the results are presented in Figure 9.

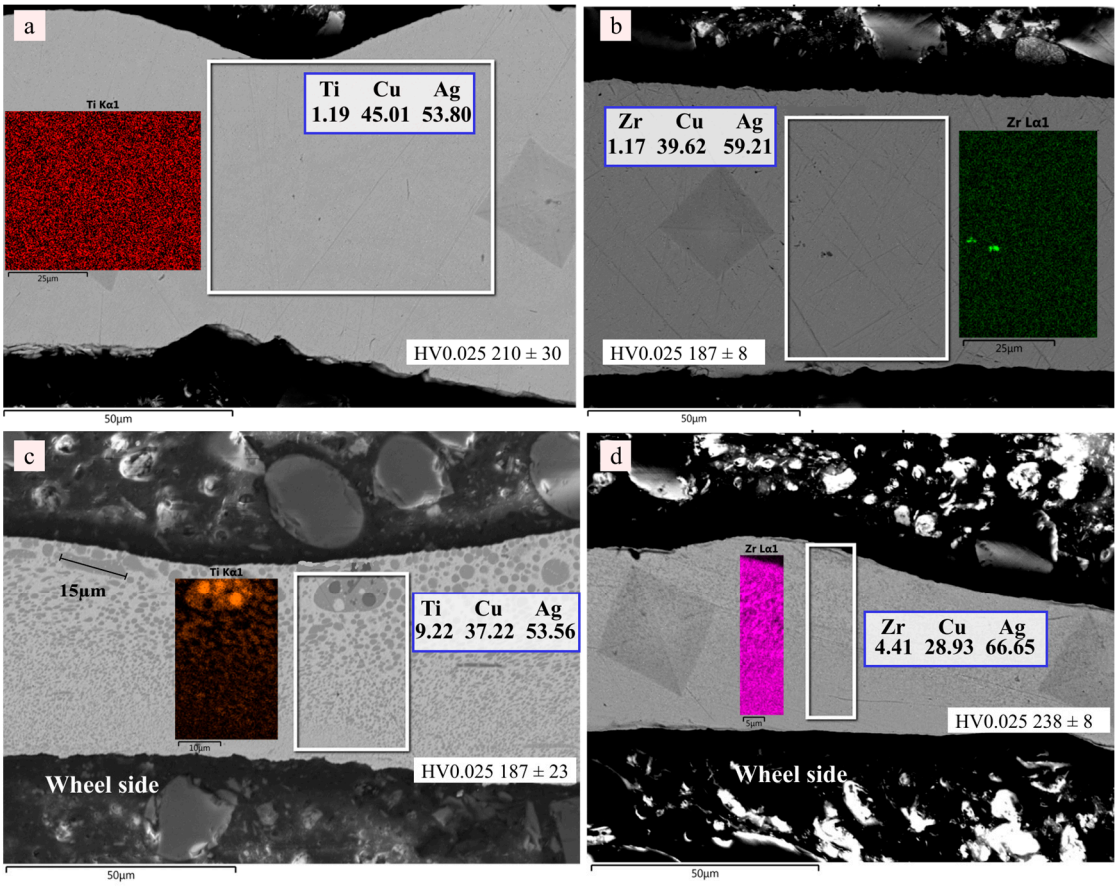

Figure 9. Microstructure of the cross section of the obtained ribbons: (**a**)—AgCu1.5Ti; (**b**)—AgCu1.5Zr; (**c**)—AgCu5Ti; (**d**)—AgCu5Zr.

Figure 9 shows that the ribbons containing 1.5 wt.% of the active element (Figure 9a,b) have a more homogeneous structure, and their elemental composition is close to the nominal one. It is also noted that rapid quenching leads to significant refinement of the intermetallic phases. In the brazing ribbons with an alloying element content of 5 wt.% (Figure 9c,d), an increase in phase size was observed with increasing distance from the wheel side. The AgCu5Ti ribbon contains relatively large inclusions, reaching up to 13 μm. At the same time, the phases in the center of the ribbon and closer to the free surface do not exceed 500 nm in size. It is also worth noting that the phase size in the AgCu5Zr ribbon does not exceed 500 nm throughout its entire thickness.

The melting range of the produced brazing alloys was investigated using DSC. The measurement results are presented in Table 4.

Table 4. Results of differential scanning calorimetry measurements.

Material	Liquidus, °C	Solidus, °C
AgCu1.5Zr	810	774 ± 2
AgCu5Zr	860	774 ± 2
AgCu1.5Ti	805	780 ± 2
AgCu5Ti	830	780 ± 2

The obtained values are in good agreement with the literature data and phase diagrams. These data were used to determine appropriate heating parameters for the wetting experiments. The wetting angles of the investigated brazing alloys are presented graphically in Figure 10.

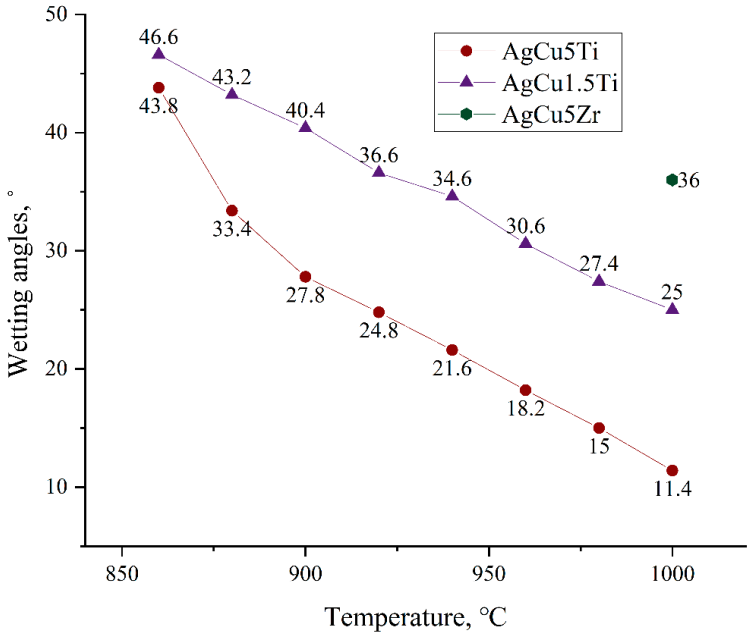

Figure 10. Wetting angles of the obtained ribbons on an alumina substrate.

The significant differences in wetting angles (Figure 10) stem from the distinct interfacial chemistry and kinetics governed by the active element (Ti or Zr) and its content. For the Ag–Cu–Ti system, both alloys exhibit excellent wettability due to the high redox activity of titanium, which reduces the Al_2O_3 surface to form titanium oxides and Cu–Ti–O intermetallic compounds at the interface. The superior performance of the AgCu5Ti ribbon ($\theta = 11.4°$), compared to AgCu1.5Ti ($\theta = 25°$), is a direct consequence of the higher thermodynamic driving force and greater Ti supply for the interfacial reaction, facilitated by the refined, homogeneous microstructure of the rapidly quenched state.

In contrast, the wetting behavior of the Ag–Cu–Zr system is governed by different kinetics. The AgCu5Zr alloy eventually wets the substrate, but with a pronounced delay, attributed to the necessary dissolution of a native ZrO_2 film on the alloy surface before active interaction with the ceramic can commence. Once this barrier is overcome at ~1000 °C, zirconium forms a ZrO_2-based layer, enabling bonding. The poor spreading of the AgCu1.5Zr composition suggests that 1.5 wt.% Zr is below a critical threshold for an effective interfacial reaction under these conditions; the limited Zr may be kinetically trapped in fine intermetallic particles within the ribbon microstructure, reducing its availability at the interface.

These findings have direct implications for brazing process design. The excellent and rapid wettability of the Ti-containing alloys, particularly AgCu5Ti, indicates that they are

suitable for efficient brazing cycles with relatively low peak temperatures (in the range of 850–900 °C, just above their liquidus) and short holding times. This enables a low-thermal-budget process, minimizing residual stresses and component degradation. For the AgCu5Zr alloy, reliable bonding requires a dedicated high-temperature cycle with a peak temperature of at least 1000 °C and a prolonged holding time to ensure dissolution of the surface oxide and subsequent interfacial reaction. Such a cycle is more energy-intensive and increases the risk of excessive brittle layer formation. Consequently, the rapidly quenched AgCu5Ti ribbon emerges as the most promising candidate, enabling a robust and economical single-step active brazing process for alumina. In contrast, the AgCu5Zr alloy may be considered for specialized high-temperature applications where the use of Ti is undesirable. The AgCu1.5Zr composition, due to its inadequate wetting, is not recommended for direct brazing of alumina under standard vacuum conditions.

4. Conclusions

This work focused on the synthesis and comprehensive characterization of rapidly quenched ribbon brazing alloys based on the Ag–Cu–Ti (Ag–26.5Cu–1.5Ti, Ag–25Cu–5Ti) and Ag–Cu–Zr (Ag–26.5Cu–1.5Zr, Ag–25Cu–5Zr) systems. The study encompassed the analysis of their microstructure, phase composition, thermal properties, mechanical characteristics, and wetting behavior on ceramic substrates to assess their potential for high-temperature metal–ceramic joining. The main findings are as follows:

(1) Homogenization annealing at 730 °C for 5 h effectively eliminated liquation inhomogeneity in all studied alloys. The microstructural transformation mechanisms include spheroidization, coagulation, and dissolution of the intermetallic phases.

(2) The optimal alloying element concentration for both systems is 1.5 wt.%. Ag–Cu–1.5Zr demonstrates $\sigma_{0.2}$ = 299 ± 24 MPa, σ_{uts} = 331 ± 21 MPa, and δ = 17.5%, with fracture occurring uniformly through intermetallics. AgCu1.5Ti shows the highest strength: $\sigma_{0.2}$ = 318.8 ± 1.7 MPa, σ_{uts} = 351.4 ± 1.5 MPa, and δ = 17.9%; however, SEM images of the fracture surfaces reveal cracked and pulled-out intermetallic particles, indicating a more brittle matrix–particle interface. Increasing the alloying element content to 5 wt.% degrades the mechanical properties, with the degradation behavior differing between the two elements. AgCu5Zr retains moderate ductility (δ = 5%) and stable strength (σ_{uts} = 258 ± 4 MPa) due to its uniform structure. In contrast, AgCu5Ti undergoes catastrophic embrittlement: σ_{uts} = 176 ± 8 MPa, δ = 2%. The $\sigma_{uts} < \sigma_{0.2}$ ratio indicates brittle failure within the elastic regime, caused by large intermetallic structures.

(3) Phase analysis confirms the multiphase nature of the ingots. AgCu5Ti contains CuTi and Cu_4Ti intermetallics, while AgCu5Zr consists of $AgCu_4Zr$ and Zr_2Cu phases. The calculated B/G ratio suggests that most observed intermetallic phases are ductile; the most brittle among them is CuTi (B/G = 1.65).

(4) Rapid quenching produces ribbons with highly refined microstructures. At 1.5 wt.% of the active element, the phase distribution is uniform across the ribbon thickness. In the AgCu5Ti ribbon, coarse inclusions up to 13 μm appear only on the wheel side, while phases in the center and near the free surface do not exceed 500 nm. The AgCu5Zr ribbon exhibits phase sizes below 500 nm throughout its entire thickness. The solidus temperatures are 774 ± 2 °C for Zr-alloyed and 780 ± 2 °C for Ti-alloyed compositions. The liquidus temperatures range from 805 °C (AgCu1.5Ti) to 860 °C (AgCu5Zr).

(5) Wetting behavior on alumina substrates is strongly governed by the type and concentration of the active element. AgCu5Ti exhibits excellent wettability (θ = 11.4°), significantly outperforming AgCu1.5Ti (θ = 25°), which is attributed to higher ti-

tanium activity and the homogeneous ribbon microstructure. AgCu5Zr wets the substrate with a pronounced delay, requiring heating to 1000 °C to break down the native ZrO_2 film; AgCu1.5Zr shows poor spreading, indicating that 1.5 wt.% Zr is insufficient for an effective interfacial reaction under the studied conditions.

In summary, the rapidly quenched ribbons AgCu1.5Ti, AgCu5Ti, and AgCu5Zr demonstrate promising characteristics for producing heat-resistant joints. The results establish a foundation for the next research phase: fabricating and testing brazed joints to evaluate their mechanical strength and thermal shock resistance under cyclic loading conditions.

Author Contributions: Conceptualization, A.I. and S.T.; methodology, A.I. and S.T.; software, A.A. and V.K.; formal analysis, V.M. and A.B.; investigation, I.K., N.P. and P.M.; resources, I.F.; writing—original draft preparation, S.T.; writing—review and editing, A.I. and S.T.; visualization, S.T.; supervision, O.S.; project administration, O.S.; funding acquisition, A.I. All authors have read and agreed to the published version of the manuscript.

Funding: The research was carried out at the expense of a grant from the Russian Science Foundation №. 25-19-00778, https://rscf.ru/project/25-19-00778/ (accessed on 1 November 2025).

Data Availability Statement: Data is contained within the article.

Acknowledgments: During the preparation of this manuscript, the authors used DeepSeek-V3.2 for the purposes of proofreading and editing. The authors have reviewed and edited the output and take full responsibility for the content of this publication.

Conflicts of Interest: The authors declare no conflicts of interest.

References

1. Vianco, P.T. A Review of Interface Microstructures in Electronic Packaging Applications: Brazing and Welding Technologies. *JOM* **2022**, *74*, 3557–3577. [CrossRef]
2. Klomp, J.T.; de With, G. Strong Metal-Ceramic Joints. *Mater. Manuf. Process.* **1993**, *8*, 129–157. [CrossRef]
3. Sekulić, D.P. (Ed.) *Advances in Brazing: Science, Technology and Applications*; Elsevier: Oxford, UK, 2013.
4. Mishra, P.; Kumar, V.; Yadav, V.; Ghosh, S.; Tiwari, S.; Singh, A.; Dutta, M.; Ghosh, R.N. Brazing of Hot Isostatically Pressed–Al_2O_3 to Stainless Steel (AISI 304L) by Mo-Mn Route Using 72Ag-28Cu Braze. *Metall. Mater. Trans. A* **2005**, *36*, 1487–1499. [CrossRef]
5. Mishra, S.; Sharma, A.; Jung, D.-H.; Jung, J.P. Recent Advances in Active Metal Brazing of Ceramics and Process. *Met. Mater. Int.* **2020**, *26*, 1087–1098. [CrossRef]
6. Naidich, Y.V.; Zhuravlev, V.S.; Gab, I.I.; Krasovskaya, N.V.; Kurkova, D.I.; Bogomol, I.V. Liquid Metal Wettability and Advanced Ceramic Brazing. *J. Eur. Ceram. Soc.* **2008**, *28*, 717–728. [CrossRef]
7. Loehman, R.E.; Tomsia, A.P. Reactions of Ti and Zr with AlN and Al_2O_3. *Acta Metall. Mater.* **1992**, *40*, S75–S83. [CrossRef]
8. Hao, H.; Jin, Z.; Wang, X. The Influence of Brazing Conditions on Joint Strength in Al_2O_3/Al_2O_3 Bonding. *J. Mater. Sci.* **1994**, *29*, 5041–5046. [CrossRef]
9. Mandal, S.; Ray, A.K.; Ray, A.K. Correlation between the Mechanical Properties and the Microstructural Behaviour of Al_2O_3-(Ag-Cu-Ti) Brazed Joints. *Mater. Sci. Eng. A* **2004**, *383*, 235–244. [CrossRef]
10. Wen, Y.; Zhang, S.; Huang, W.; Yu, D.; Hu, L.; Wang, P.; Fang, R.; Ouyang, P. Effect of Ti content on microstructure and properties of Cu/AgCuTi/Al_2O_3 brazed joints. *Mater. Today Commun.* **2024**, *40*, 109507. [CrossRef]
11. Zaharinie, T.; Huda, Z.; Ibrahim, S.; Yusof, F.; Hamdi, M.; Rehan, M.; Ariga, T. Analysis of the Reaction Layer Formed during Sapphire–Sapphire Brazing Using a Ag–Cu–Ti Filler Metal for Gas-Pressure Sensors. *ACS Appl. Electron. Mater.* **2022**, *4*, 2405–2412. [CrossRef]
12. Zhu, Q.; Cai, Y.; Liu, Z.; Gong, K.; Wang, Z.; Li, L.; Zhang, Y. Brazing Al_2O_3 to 4J42 using Ag–Cu–Ti/Cu/BNi-2 composite fillers with different thicknesses of Cu interlayer. *Ceram. Int.* **2023**, *49*, 9779–9788. [CrossRef]
13. Kim, J.-H.; Yoo, Y.-C. Bonding of Alumina to Metals with Ag-Cu-Zr Brazing Alloy. *J. Mater. Sci. Lett.* **1997**, *16*, 1212–1215. [CrossRef]
14. Stephens, J.J.; Burchett, S.N.; Hosking, F.M. The Evolution of a Ternary Ag-Cu-Zr Active Braze Filler Metal for Kovar™/Alumina Braze Joints. In Proceedings of the 3rd International Brazing and Soldering Conference, San Diego, CA, USA, 24–26 April 2006; pp. 207–213.
15. Yoo, Y.C.; Kim, J.H.; Park, K. Microstructure and Bond Strength of Ni–Cr Steel/Al_2O_3 Joints Brazed with Ag–Cu–Zr Alloys Containing Sn or Al. *Mater. Sci. Technol.* **1999**, *15*, 1331–1334. [CrossRef]

16. Yoo, Y.C.; Kim, J.H.; Park, K. Microstructural Characterization of Al_2O_3/AISI 8650 Steel Joint Brazed with Ag–Cu–Sn–Zr Alloy. *Mater. Lett.* **2000**, *42*, 362–366. [CrossRef]
17. Mohammed Jasim, K.; Rawlings, R.D.; West, D.R.F. Actively Brazed Alumina to Alumina Joints Using CuTi, CuZr and Eutectic AgCuTi Filler Alloys. *Ceram. Int.* **2010**, *36*, 2287–2295. [CrossRef]
18. Hatami Ramsheh, H.; Simchi, A.; Kokabi, A.H. Microstructure and Mechanical Properties of $MoSi_2$–$MoSi_2$ Joints Brazed by Ag–Cu–Zr Interlayer. *Mater. Des.* **2013**, *49*, 197–202. [CrossRef]
19. Rajendran, S.H.; Hwang, S.J.; Jung, J.P. Active Brazing of Alumina and Copper with Multicomponent Ag-Cu-Sn-Zr-Ti Filler. *Metals* **2021**, *11*, 509. [CrossRef]
20. Raghava Simhan, D.; Mukhopadhyay, P.; Ghosh, A. On Segregation of Zr and Wettability of Active Ag-Cu-Zr Alloy on Cubic Boron Nitride Surface. *Mater. Lett.* **2017**, *207*, 183–186. [CrossRef]
21. Raghava Simhan, D.; Ghosh, A. Vacuum Brazing of Cubic Boron Nitride to Medium Carbon Steel with Zr Added Passive and Ti Activated Eutectic Ag-Cu Alloys. *Ceram. Int.* **2018**, *44*, 7149–7162. [CrossRef]
22. Janičkovič, D.; Šebo, P.; Duhaj, P.; Švec, P. The rapidly quenched Ag-Cu-Ti ribbons for active joining of ceramics. *Mater. Sci. Eng. A* **2001**, *304*, 569–573. [CrossRef]
23. Ziewiec, K.; Kędzierski, Z.; Zielińska-Lipiec, A.; Stępiński, J.; Kąc, S. Formation, properties and microstructure of amorphous/crystalline composite Ag20Cu30Ti50 alloy using miscibility gap. *J. Alloys Compd.* **2009**, *482*, 114–117. [CrossRef]
24. Castellero, A.; Angella, G.; Vedani, M.; Baricco, M. Rapid solidification of silver-rich Ag–Cu–Zr–Al alloys. *J. Alloys Compd.* **2014**, *586*, S111–S116. [CrossRef]
25. Ivannikov, A.A.; Logvenchev, I.S.; Kalin, B.A.; Fedotov, I.V.; Sevryukov, O.N.; Korshunov, A.V. Rapid-Quenched Nickel-Based Solder for High-Temperature Brazing of Various Constructive Elements. *Tsvetnye Met.* **2014**, *12*, 27–31.
26. Logvenchev, I.S.; Ivannikov, A.A.; Kalin, B.A.; Sevryukov, O.N.; Fedotov, I.V.; Korshunov, A.V.; Suchkov, A.N. The Brazing of Nickel Alloys for Nuclear Reactor with the Using of the Rapidly-Quenched Filler Metals. *Inorg. Mater. Appl. Res.* **2014**, *5*, 240–244. [CrossRef]
27. Wang, J.L.; Wu, L.Z.; Ma, K.; Liu, B.; Xiong, H.P. Microstructural Stability and Mechanical Properties of Al_2O_3/Kovar 4 J34 Joint Vacuum Brazed Using Ag-5Cu-1Al-1.25Ti (wt%) Filler Metal. *J. Manuf. Process.* **2021**, *72*, 553–564. [CrossRef]
28. Zhu, Q.; Wang, J.; Xiong, H.; Sun, G.; Cheng, H.; Wu, L. Enhanced Mechanical Properties and Thermal Cycling Stability of Al_2O_3-4J42 Joints Brazed Using Ag–Cu–Ti/Cu/Ag–Cu Composite Filler. *Ceram. Int.* **2021**, *47*, 30247–30255. [CrossRef]
29. Terekhova, S.M.; Boldin, A.A.; Chernyavtsev, D.A.; Raevskaya, E.G.; Stepnov, K.K. Thermal Stability of Metal-Ceramic Kovar®/94% Alumina Joints. *Ceram. Int.* **2025**, *51*, 59452–59461. [CrossRef]
30. Qi, J.; Zhu, Q.; Han, S.; Chen, S.; Wu, L.; Wang, J. Study on the Layered Structure of Ceramic-Side Bonding Area and the Mechanical Property of Al_2O_3–Kovar Brazed Joint with Ag-Cu-Ti Filler. *J. Manuf. Mater. Process.* **2025**, *9*, 355. [CrossRef]
31. Irmagambetova, S.M.; Ermakov, S.A.; Glushenkov, A.E.; Torgunaev, D.A.; Egorov, A.A. Vliyanie razmerov i formy ploskikh obraztsov na opredelyaemye kratkovremennye mekhanicheskie svoistva materialov [The effect of the size and shape of flat samples on the determined short-term mechanical properties of materials]. *Vopr. At. Nauki Tekh.* **2025**, *2*, 18–24.
32. *GOST 23904-79*; Brazing and Soldering. Method for Determination of Materials Wetting with Solders. Izdatel'stvo Standartov: Moscow, Russia, 1982.
33. Zhu, Y.D.; Yan, M.F.; Zhang, Y.X.; Zhang, C.S. First-principles investigation of structural, mechanical and electronic properties for Cu–Ti intermetallics. *Comput. Mater. Sci.* **2016**, *123*, 70–78. [CrossRef]
34. Cora, I.; Pekker, P.; Dódony, I.; Janovszky, D. Single crystal structure determination and refinement of $AgZrCu_4$ and Ag-containing $Cu_{10}Zr_7$ by precession electron diffraction and tomography techniques. *J. Alloys Compd.* **2016**, *658*, 678–683. [CrossRef]
35. Du, J.; Wen, B.; Melnik, R.; Kawazoe, Y. Phase stability, elastic and electronic properties of Cu–Zr binary system intermetallic compounds: A first-principles study. *J. Alloys Compd.* **2014**, *588*, 96–102. [CrossRef]
36. Xu, Y.; Tian, M.; Hu, C.; Han, Z.; Zhou, S.; Cao, Y. Structural, electronic, mechanical, and thermodynamic properties of Cu–Ti intermetallic compounds: First-principles calculations. *Solid State Commun.* **2022**, *352*, 114814. [CrossRef]